

Effects of lattice disorder in the $\text{UCu}_{5-x}\text{Pd}_x$ system

E. D. Bauer,¹ C. H. Booth,² G. H. Kwei,^{3,4} R. Chau,³ and M. B. Maple¹

¹*Department of Physics and Institute For Pure and Applied Physical Sciences,
University of California, San Diego, La Jolla, CA 92093, USA*

²*Chemical Sciences Division, Lawrence Berkeley National Laboratory, Berkeley, California 94720, USA*

³*Lawrence Livermore National Laboratory, Livermore, California, 94550, USA*

⁴*Los Alamos National Laboratory, Los Alamos, New Mexico, 87545, USA*

(Dated: preprint, March 29, 2002)

The $\text{UCu}_{5-x}\text{Pd}_x$ system exhibits non-Fermi liquid (NFL) behavior in thermodynamic and transport properties at low temperatures for Pd concentrations $0.9 \lesssim x \lesssim 1.5$. The local structure around the U, Cu, and Pd atoms has been measured for $0 \leq x \leq 1.5$ using the x-ray absorption fine structure (XAFS) technique in order to quantify the effects of lattice disorder on the NFL properties. A model which allows a percentage of the Pd atoms to occupy nominal Cu (16e) sites, s , was used to fit the Pd and Cu K edge and U L_{III} edge data. Pd/Cu site interchange was found to occur in all samples ($x \neq 0$), reaching a minimum value of $s \sim 0.17$ at $x = 0.7$ and increasing monotonically to $s \simeq 0.4$ at $x = 1.5$. These data also determine an upper limit on the static disorder of the nearest neighbor U-Cu pairs. A single-ion Kondo disorder model with a lattice-disorder origin of the distribution of f /conduction electron hybridization strengths within a tight-binding approach is used to calculate magnetic susceptibility. The results indicate that the measured U-Cu static disorder is not sufficient to explain the NFL behavior of the magnetic susceptibility within this variant of the Kondo disorder model, suggesting either that other sources of Kondo disorder exist or that the Kondo disorder model is not applicable to $\text{UCu}_{5-x}\text{Pd}_x$.

PACS numbers: 72.15.Qm, 61.10.Ht, 71.23.-k, 71.27.+a

I. INTRODUCTION

In f -electron compounds, strong electronic correlations lead to a variety of interesting ground states. Recently, there has been growing interest in heavy fermion compounds that display non-Fermi liquid (NFL) behavior in which the low temperature properties, such as the electronic specific heat coefficient $C(T)/T \equiv \gamma$, magnetic susceptibility $\chi(T)$, and electrical resistivity $\rho(T)$, are characterized by logarithmic or power law temperature dependences. These characteristic temperature dependences are in contrast to those of a Fermi liquid in which $\gamma \sim \chi \sim \text{constant}$, and $\rho(T) \propto T^2$ at low temperatures.¹ The NFL behavior of many of these Ce-, Yb-, or U-based heavy fermion materials is often observed when long range magnetic order is suppressed by the substitution of a nonmagnetic element or by the application of pressure (for a review, see Refs. 2,3,4,5,6).

There have been a number of theories proposed to account for non-Fermi liquid behavior, although in many cases, several models adequately describe the low temperature properties, making an unambiguous choice of theories difficult. In some systems, the NFL properties may be associated with the proximity to a $T = 0$ K second order phase transition or quantum critical point (QCP).^{7,8,9} Since many materials that display non-Fermi liquid phenomena are disordered alloys, various disorder-driven mechanisms have also been proposed. The “Kondo disorder” model (KDM)^{10,11,12} is essentially a single-impurity model with a distribution of Kondo temperatures, and might be considered as a disordered Fermi liquid model. The KDM utilizes a dis-

tribution of Kondo temperatures T_K caused by a distribution of f -electron/conduction electron exchange coupling strengths \mathcal{J} , possibly induced by lattice disorder. This model was first put forth to explain the broad NMR linewidths and muon spin rotation measurements on UCu_4Pd .^{10,13} Measurements of electrical resistivity, specific heat, and magnetic susceptibility are also consistent with this model.^{14,15} Castro Neto *et al.* proposed a model^{16,17} which describes the competition between the RKKY and Kondo interactions in a disordered material leading to the formation of magnetic clusters similar to a Griffiths’ phase.¹⁸ This theory predicts that the physical properties of the system at low temperatures are characterized by weak power law behavior and is consistent with what is observed experimentally in a number of NFL materials.^{19,20} Recently, Miranda and Dobrosavljević investigated a disordered Anderson lattice and proposed that a Griffiths’ phase could be obtained by a disorder-driven metal-insulator transition (MIT).^{21,22}

It is essential to determine the nature of the lattice disorder in these disordered non-Fermi liquid systems, since it is a key ingredient in many of the theories put forth and, therefore, may provide valuable information regarding the underlying mechanism for the NFL behavior. The $\text{UCu}_{5-x}\text{Pd}_x$ system was chosen for this investigation because of its rich phase diagram and because one type of disorder, Pd/Cu site interchange, in which Pd ions occupy nominal Cu (16e) sites, was found to be relevant to the NFL properties at low temperatures for UCu_4Pd .²³ Lattice disorder has also been shown to be important from changes in the lattice parameter and γ in annealing studies of UCu_4Pd (Ref. 24) and the Cu-NQR line-shape in $\text{UCu}_{3.5}\text{Pd}_{1.5}$,²⁵ and is implied from the glassy

nature of the spin dynamics measured from the muon spin-lattice relaxation.²⁶ The details of the low temperature magnetic phase diagram are much more complicated than originally believed. In $\text{UCu}_{5-x}\text{Pd}_x$, antiferromagnetic order is suppressed from $T_N = 15$ K in UCu_5 , to $T = 0$ K at $x \sim 1$.^{14,15} Although no frozen moments are observed from muon spin-relaxation,²⁶ glassy behavior (spin glass or superparamagnetism) is observed for $x = 1$ at $T_f \sim 0.2$ K, while no evidence for magnetic order down to 30 mK is found for $x = 1.25$.^{20,27} For $x = 1.5$, spin glass behavior reappears at $T_f \sim 0.1$ K which persists up to $x = 2.2$ ($T_f \sim 2$ K), at which point the system enters into a mixed phase region with two different crystal structures. Therefore, the $\text{UCu}_{5-x}\text{Pd}_x$ system offers an opportunity to study the effects of disorder on the relevant physical properties (i.e., magnetic order, NFL behavior, etc.). In addition, it is still an open question as to which model for non-Fermi liquid behavior is most appropriate for this system. A quantum critical point may exist given the absence of magnetic order of any kind at $x = 1.25$. The various Griffiths' phase models^{16,21} may be applicable since disorder is present in this system.²³ The Kondo disorder scenario may also be valid as many of the physical properties are consistent with this model.^{10,13,15}

The main motivations for this study are: (1) to determine the amount of lattice disorder in $\text{UCu}_{5-x}\text{Pd}_x$; (2) to calculate the distribution of hybridization strengths $P(V)$ using the measured lattice disorder; (3) to test the caveat of lattice disorder as a possible starting point for a true microscopic model of the Kondo disorder model proposed in a previous study of Pd/Cu site interchange in UCu_4Pd ;²³ (4) and, finally, to speculate on the applicability of models other than the KDM to describe the NFL behavior of $\text{UCu}_{5-x}\text{Pd}_x$. The x-ray absorption fine-structure (XAFS) technique is a powerful tool for studying disorder since it is a local structural probe that is atomic species specific. We will present a method for quantitatively determining the amount of disorder around the U atoms in the $\text{UCu}_{5-x}\text{Pd}_x$ system. This method can be applied to many systems in which it is helpful to understand the nature of the disorder (or lack thereof) and its relation to the physical properties.

The outline of the paper is as follows: experimental details and a brief description of the XAFS technique are discussed in Sec. II. The theoretical background for the KDM along with fits of this model to the magnetic susceptibility are presented in Sec. III. The experimental analysis methods, Pd and Cu K edge and U L_{III} edge XAFS data and results from $\text{UCu}_{5-x}\text{Pd}_x$ ($0 \leq x \leq 1.5$) samples are given in Sec. IV. The effects of the measured lattice disorder on the electronic properties of the $\text{UCu}_{5-x}\text{Pd}_x$ system are considered in Sec. V. A discussion of the results are presented in Sec. VI and conclusions are given in Sec. VII.

II. EXPERIMENTAL DETAILS

Samples of $\text{UCu}_{5-x}\text{Pd}_x$ were prepared by arc melting appropriate amounts of the end members UCu_5 and UPd_5 in an ultra high purity Ar atmosphere with a Zr getter. The parent compound UCu_5 was annealed in an evacuated quartz ampoule at 900°C for 2 weeks, while no annealing was performed on the compounds containing Pd. All of the materials were found to be single phase with the AuBe_5 crystal structure with no observable impurity peaks according to x-ray diffraction measurements. A slightly Cu deficient sample, with composition $\text{UCu}_{4.95}$, was also prepared in order to minimize Cu inclusions.²⁸ However, the behavior of UCu_5 and $\text{UCu}_{4.95}$ were very similar and only the data for the UCu_5 compound is reported except where otherwise noted. Magnetic susceptibility measurements were performed in a commercial SQUID magnetometer in a magnetic field of 1 tesla at temperatures between 1.8 K and 300 K.

X-ray absorption data were collected at the Stanford Synchrotron Radiation Laboratory from the U L_{III} , Pd K , and Cu K edges on BL 4-3 and BL 10-2 using a half-tuned double crystal Si(220) monochromator with a slit height of 0.7 mm. The samples were ground to a fine powder in acetone, passed through a 30 micron sieve, and brushed onto scotch tape. Since UCu_5 oxidizes rapidly,²⁹ such powder samples were prepared in an Ar glove box and sealed between layers of capton tape and shipped in a quartz tube filled with Ar. The capton-sealed UCu_5 and $\text{UCu}_{4.95}$ samples were exposed to air for less than ten minutes while being loaded into the cryostat. Various numbers of layers were stacked so that the edge step was approximately unity for each type of edge. Generally, 2-5 scans were collected for each sample for a particular edge at temperatures between 3 K and 300 K with a temperature deviation of less than 0.2 K.

The absorption data were reduced using standard procedures outlined in Refs. 30 and 31, including fitting an embedded-atom absorption function $\mu_0(E)$ with a 5-7-knot cubic spline function with a maximum photoelectron wavevector k of 15 \AA^{-1} . The XAFS function is then defined as $\mu(k)/\mu_0(k) - 1$, where μ is the absorption coefficient, $k = \sqrt{\frac{2m_e}{\hbar^2}(E - E_0)}$ is the photoelectron wavevector, m_e is the electron rest mass, and E_0 is the absorption edge threshold energy, which is defined arbitrarily to be the half-height of the edge and allowed to vary in the fits. Examples of the k -space data for each of the absorption edges are shown in Fig. 1.

The XAFS technique provides local structural information about an absorbing atom. The oscillation above an absorption edge, which are due to the interference between the outgoing and backscattered photoelectron waves, can be Fourier transformed and subsequently fit in order to determine the following quantities: N_i , the number of atoms in the i^{th} shell at a radius R_i from the absorbing atom; σ_i , the spread in bond lengths at R_i (also called the Debye-Waller factor); and S_0^2 , an overall am-

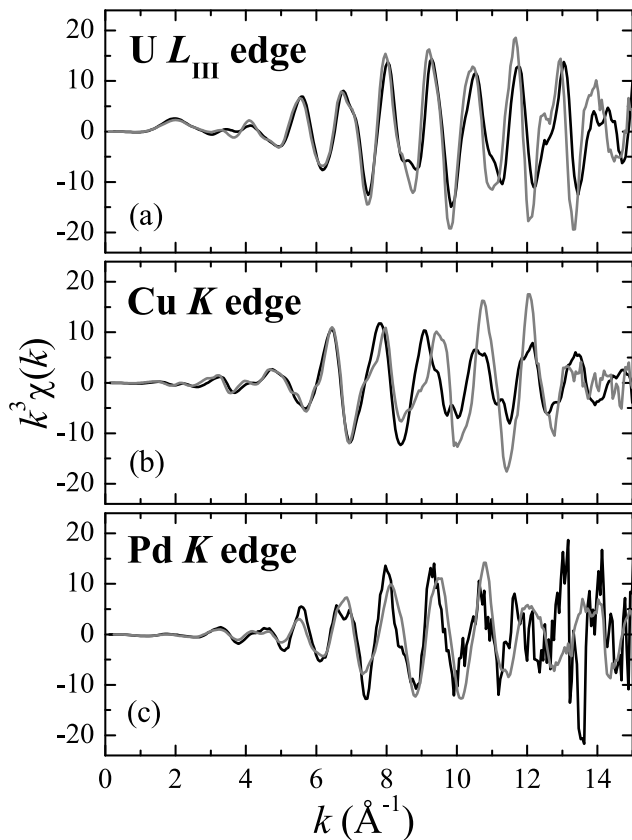


Fig. 1, E.D. Bauer et al.

FIG. 1: Examples of the $k^3\chi(k)$ XAFS data for the $x=0.3$ (dark) and the $x=1.5$ (light) samples from the (a) U L_{III} , (b) Cu K , and (c) Pd K edges. Note the relatively poor quality of the Pd K edge data for $x=0.3$. The data quality of other samples is similar to that of the $x=1.5$ sample.

plitude reduction factor that accounts for inelastic losses. Theoretical predictions for S_0^2 generally do not compare well with experiment; therefore, N_i is held fixed whenever possible. In this study, we fit the Fourier Transform (FT) of the XAFS function $k^3\chi(k)$ to the theoretical backscattering and phase functions calculated by FEFF7³² (more details can be found in Ref. 31). The absolute errors in σ are estimated to be 5% for nearest neighbor bonds and 10% for further neighbor bonds. The absolute errors in R are estimated to be 0.01 Å for nearest neighbor bonds and 0.02 Å for further neighbor bonds.³¹ These absolute error estimates are similar to (though always larger than) those obtained by other methods such as a Monte Carlo method³³ or the relative errors estimated from the number of scans taken at a given temperature for all the measurements report here.

As an additional check on the sample purity of the $UCu_{5-x}Pd_x$ samples, a contribution to the XAFS of a number of impurities were considered such as Cu, Pd, CuPd, Cu_3Pd , as well as various oxides. Simulations of the XAFS spectra expected from nearly all of these impurity compounds indicated that the tested impuri-

ties would produce peaks that were not observed in the $UCu_{5-x}Pd_x$ data and therefore these impurities could only be present at levels of less than a few percent. The impurity level of compounds with similar crystal structures and lattice parameters, such as free Cu (which was reported to exist in $UCu_{4.35}Pd_{0.65}$ (Ref. 34)), could be as high as 5%.

III. BACKGROUND

A. Magnetic susceptibility and logarithmic behavior

Measurements of magnetic susceptibility were performed in order to track the decrease of the Néel temperature with increasing Pd concentration and to explore the non-Fermi liquid behavior observed previously.^{14,15} The magnetic susceptibility $\chi \equiv M/H$ vs temperature T in a magnetic field of $H = 1$ T for various $UCu_{5-x}Pd_x$ compounds is shown in Fig. 2. A cusp or peak of the $\chi(T)$ curves is observed for $0 \leq x \leq 0.7$, indicating the onset of antiferromagnetic order at $T_N = 15.5$ K, 14.1 K, 8.4 K, and 2.3 K for $x=0, 0.3, 0.5$, and 0.7 , respectively, in agreement with previous results.^{14,15} For $0.9 \leq x \leq 1.5$, the $\chi(T)$ data increases with decreasing temperature at low T and can be fitted by the expressions $\chi(T) = \chi_0 - c \ln T$ where χ_0 and c are constants, or $\chi(T) = -c'T^n$ where c' is a constant and n ranges between -0.2 and -0.3, as shown in the inset of Fig. 2. Similar power law behavior has been previously observed in $UCu_{5-x}Pd_x$ (Ref. 20) and other disordered NFL systems such as $Y_{1-x}U_xPd_3$ and $Th_{1-x}U_xPd_2Al_3$.¹⁹ At higher temperatures above ~ 200 K, the magnetic susceptibility of the $UCu_{5-x}Pd_x$ compounds follows a Curie-Weiss law:

$$\chi = C/(T - \theta_{CW})$$

where $C = N_A\mu_{eff}^2/3k_B$, θ_{CW} is the Curie-Weiss temperature and μ_{eff} is the effective moment in Bohr magnetons. The effective moment $\mu_{eff} = 3.0 - 3.4 \mu_B$ is smaller than what would be expected for a $5f^2$ ($\mu_{eff} = 3.58 \mu_B$) or $5f^3$ ($\mu_{eff} = 3.62 \mu_B$) configuration, indicating the presence of crystalline electric field effects and/or the Kondo effect. The Curie-Weiss temperatures θ_{CW} are negative for all concentrations studied and increase roughly linearly from -260 K to -100 K from $x = 0.3$ to $x = 1.5$ (results listed in Table I).

B. Lattice disorder and the KDM

In the Kondo disorder model, a logarithmic divergence at low temperatures in the magnetic susceptibility $\chi(T)$ and specific heat divided by temperature $C(T)/T$ are produced when a sufficient amount of weight in the distribution of Kondo temperatures $P(T_K)$ exists at low- T_K .¹⁰ The $P(T_K)$ distribution is determined by introducing a

TABLE I: Magnetic properties of $\text{UCu}_{5-x}\text{Pd}_x$. The Néel temperature T_N is obtained from the change in slope of the $\chi(T)$ curves. The values of the effective moment μ_{eff} and Curie-Weiss temperature θ_{CW} are extracted from fits to a Curie-Weiss law of the high temperature magnetic susceptibility. The parameters χ_0 and c are determined from fits of the expression $\chi(T) = \chi_0 - c \ln T$ to the $\chi(T)$ data. The exponent n is determined from fits of the expression $\chi(T) \propto T^n$ to the $\chi(T)$ data. The values of the static disorder necessary to fit the magnetic susceptibility σ_{KDM} are determined from fits of the KDM to the $\chi(T)$ data, and include the Cu and Pd site distributions involving the Pd concentration x and the site interchange s , as discussed in Sec. IV B.

x	T_N (K)	T_f (K)	μ_{eff} (μ_B)	θ_{CW} (K)	χ_0 ($10^{-3} \text{ cm}^3/\text{mol}$)	c ($10^{-3} \text{ cm}^3/\text{mol ln K}$)	n	σ_{KDM}^2 (\AA^2)
0	15.5		3.1	-186				
0.3	14.1		3.4	-259				
0.5	8.4		3.3	-198				
0.7	2.3		3.3	-162				
0.9	0.5 ^a		3.2	-134	23	4.9	-0.29	0.0038
1.0	0.2 ^b	0.2 ^c	3.2	-139	20	3.3	-0.26	0.0030
1.25			3.0	-97	21	2.8	-0.18	0.0028
1.5		0.1 ^d	3.2	-107	26	4.3	-0.21	0.0028

^aRef. 35

^bRef. 35

^cRef. 20,27,35

^dRef. 20,27

spread of coupling strengths, $\mathcal{J}N(E_F)$, into the expression for the Kondo temperature

$$k_B T_K = E_F e^{-1/\mathcal{J}N(E_F)} \quad (1)$$

where k_B is Boltzmann's constant, \mathcal{J} is the local moment/conduction electron exchange parameter and $N(E_F)$ is the electronic density of states of the host material at the Fermi level E_F . The exchange parameter is given by:

$$\mathcal{J} = -\frac{V_{tot}^2}{|\epsilon_f|}, \quad (2)$$

where V_{tot} is the matrix element which admixes the local moment and conduction electron states, and ϵ_f is the f -ion energy below the Fermi level.

The variant of the Kondo disorder model considered here utilizes a tight binding approach to compute the hybridization strengths V between the conduction electron states and the f -states. Since the d -electron contribution is known to dominate the conduction band in isostructural YbAgCu_4 ,³⁶ we only consider the V_{fd} matrix element. The tight binding formalism of Harrison and Straub for each pair of atoms U (f ion) and X (d electrons in the conduction band) then gives:³⁷

$$V_{fd} = \frac{\eta_{fd} \hbar^2}{m_e} \frac{\sqrt{(r_{Uf}^5 r_{Xd}^3)}}{R_{U-X}^6}, \quad (3)$$

where r_{Xl} is the radius of the electronic shell of atom X with angular momentum l ($=d$ or f) (tabulated in Ref. 38), R_{U-X} is the bond length between the U and X atoms, and η_{fd} is a factor which only depends on the l 's and bond symmetry (see Appendix B of Ref. 37). The total coupling energy is obtained by summing over

all atoms pairs

$$V_{tot} = \sum_{U,X \text{ Pairs}} V_{fd}. \quad (4)$$

Within this approach, the coupling energies are often larger than experimentally observed energies by a factor of two.³⁷ This limitation does not play a major role in what follows because these energies are scaled by $N(E_F)/\epsilon_f$, which is used as a fitting parameter. Therefore, we only need consider relative changes in V_{fd} . The sum in Eq. 4 converges rapidly since the contribution from more distant neighbors is small, i.e., $V_{fd}(R_{U-Cu} = 4.59 \text{ \AA}) \sim 7\%$ of $V_{fd}(R_{U-Cu} = 2.93 \text{ \AA})$; therefore, we assume that only the first two nearest neighbor shells contribute to the hybridization.

We include two types of contributions to the distribution of hybridization strengths due to lattice disorder. One effect is that of Pd/Cu site interchange, which changes the species of atoms used in the r_{Xd} parameters and will result in different hybridization strengths, i.e., the hybridization will be larger for a U atom with more Pd neighbors than one with more Cu neighbors. The distribution of hybridization strengths due to the different r_{Xd} parameters is therefore discrete and modeled by a binomial distribution. The other contribution to $P(V)$ is due to continuous lattice disorder, which is included as a Gaussian distribution of bond lengths R_{U-X} with width σ_{static} . The distribution of Kondo temperatures is calculated with the use of the distribution of hybridization strengths $P(V)$ in Eq. 2. With increasing continuous disorder, σ_{static} , the initial discrete $P(T_K)$ is quickly washed out even for small amounts of disorder $\sigma_{static} \sim 0.005 \text{ \AA}$, and broadens considerably with more weight shifting to lower T_K .³⁹ Sources of Kondo disorder other than a bond length distribution in the hybridization energy such as a distribution of f -ion energies or density of states $N(E_F)$

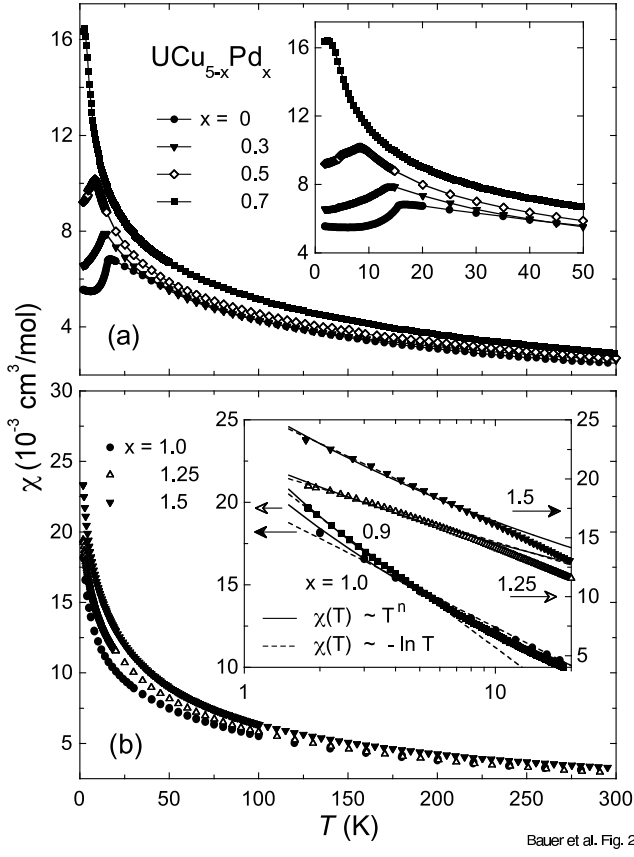


FIG. 2: Panel a): Magnetic susceptibility $\chi \equiv M/H$ vs temperature T of $\text{UCu}_{5-x}\text{Pd}_x$ compounds with Pd concentrations in the range $0 \leq x \leq 0.7$ in a magnetic field $H=1$ T. Inset: $\chi(T)$ below 50 K. Panel b): Magnetic susceptibility $\chi(T)$ in $H=1$ T for $\text{UCu}_{5-x}\text{Pd}_x$ compounds with Pd concentrations in the range $1.0 \leq x \leq 1.5$. Inset: $\chi(T)$ at low temperature for Pd concentrations between $x = 0.9$ and 1.5 . The lines are fits of the expressions $\chi(T) = \chi_0 - c \ln T$ (dashed lines) and $\chi(T) \propto T^n$ (solid lines) to the $\chi(T)$ data.

are not included in this model.

C. Fits of the KDM to the magnetic susceptibility

The magnetic susceptibility was calculated within the KDM by convolving $P(T_K)$ with the theoretical $\chi(T, T_K)$ proposed by Rajan⁴⁰ for a $J=3/2$ Kondo impurity. Three parameters were used to fit the model to the data: continuous static disorder σ_{KDM} , E_F , and $N(E_F)/\epsilon_f$. The latter two variables were found to be roughly constant for all concentrations at values of 1.36 eV (similar to the value of E_F of 1.41 eV used in Ref. 10 (for $x = 1$)) and 0.157 eV^{-2} , respectively. Least-squares fits to the $\chi(T)$ data are shown in Fig. 3 (results collected in Table I). The fit quality is excellent, especially considering that the susceptibility was derived from a microscopic model with only three adjustable parameters and the simplifying assumptions of the tight binding model

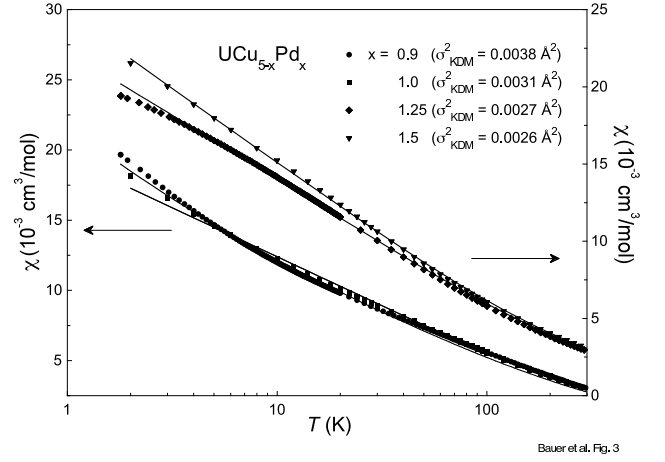


FIG. 3: Fits of the Kondo disorder model to the $\chi(T)$ data of $\text{UCu}_{5-x}\text{Pd}_x$ for Pd concentrations between $x = 0.9$ and $x = 1.5$.

and single-ion behavior. Note that, for instance, a value of $\sigma_{KDM}^2 \sim 0.0031 \text{ \AA}^2$ is necessary to produce enough weight at low T_K to generate the logarithmic divergence in $\chi(T)$ at low temperatures for the $x=1.0$ sample. The amount of static disorder used in the KDM fits decreases with increasing Pd concentration.

IV. XAFS RESULTS AND ANALYSIS

A. Experimental Analysis Procedure

Before discussing the detailed analysis procedure, it is instructive to describe the average and local structure of the $\text{UCu}_{5-x}\text{Pd}_x$ system. This system crystallizes in the face centered cubic AuBe_5 structure (C15b) for $x < 2.3$. We consider for this discussion an ordered UCu_4Pd structure in which the U and Pd atoms (4a and 4c sites, respectively) form interpenetrating FCC lattices and the Cu atoms form a network of vertex-sharing tetrahedra along the body diagonal (16e sites) as shown in Fig. 4.

The local environments of the U and Cu atoms are shown in Fig. 5a and Fig. 5b, respectively. The U and Pd environments are very similar since the U (Pd) atoms have 12 Cu neighbors at 2.93 Å and 4 Pd (U) neighbors at 3.06 Å. The local structure about the Cu atoms is different due to their tetrahedral arrangement with 6 Cu neighbors at 2.50 Å and both 3 U and Pd neighbors at 2.93 Å. The site interchange causes part of the Pd XAFS spectrum to be due to Pd atoms on 4c sites and part to be due to Pd atoms on 16e sites. The main difference between these two spectra will be due to the short Pd-Cu pair at ~ 2.5 Å arising from the Pd atoms on 16e sites.

In order to understand the effects of lattice disorder on the electronic properties in the $\text{UCu}_{5-x}\text{Pd}_x$ system, one must be able to measure the detailed local structure environment around the uranium atoms. Determining this local structure arrangement is a natural measurement

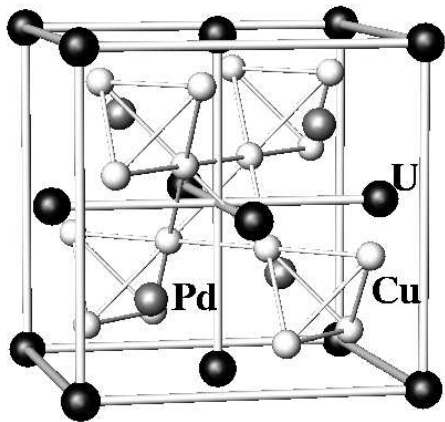


FIG. 4: Crystal structure of ordered UCu_4Pd . U atoms occupy the $4a$ sites (black spheres), Pd atoms occupy the $4c$ sites (shaded spheres), and the Cu atoms occupy the $16e$ sites (white spheres).

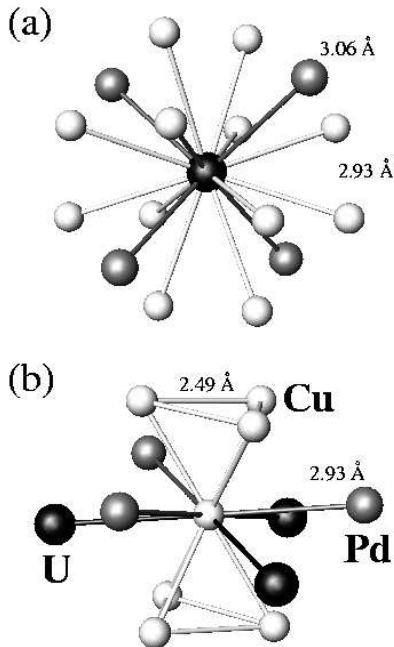


FIG. 5: Local structure in ordered UCu_4Pd . Panel a) shows the local structure about the U atoms (the Pd local structure is obtained by switching all of the U and Pd atoms). Panel b) shows the local structure about the Cu atoms.

for the XAFS technique since this technique is atomic specific, allowing the uranium atoms to be singled out. In addition, the Debye-Waller factors have been shown to be meaningful in an absolute sense, as was demonstrated for cubic materials in general,³¹ and for isostructural YbXCu_4 ($X = \text{Ag, Cd, In, Tl}$) in particular.³³ However, the presence of Pd/Cu site interchange makes the analysis procedure more complex because the species

of atom in each of the first two shells cannot necessarily be well determined in the fits to the uranium data alone.

Given the difficulty of determining the detailed local structure around the uranium atoms in $\text{UCu}_{5-x}\text{Pd}_x$, we have developed the following approach. First, we use the Pd K edge XAFS data to determine the fraction of Pd atoms on nominal Cu ($16e$) sites $s \equiv N(\text{Pd on } 16e \text{ sites})/N(\text{Total Pd})$. If, for instance, the Pd atoms are randomly distributed on all $16e$ and $4c$ sites for UCu_4Pd , the value of s would be 0.8 ($4/5$ of all possible sites are $16e$ sites). Once values of s (and errors on s) are determined, these can be held fixed in fits to the U L_{III} edge data, and a reliable value of the square of the Debye-Waller factor of the nearest-neighbor U-Cu pair $\sigma_{\text{U-Cu}}^2$ can be determined. With these values of $\sigma_{\text{U-Cu}}^2$ as a function of temperature, one may then estimate the amount of static (i.e., non-thermal) pair distance disorder by fitting the U edge data to a correlated-Debye model with a temperature-independent offset:⁴¹

$$\sigma_{\text{meas}}^2(T, \theta_{cD}) = \sigma_{\text{static}}^2 + F(T, \theta_{cD}). \quad (5)$$

The temperature-dependent part of the Debye-Waller factor $F(T, \theta_{cD})$ is given by the correlated Debye model

$$F(T, \theta_{cD}) = \frac{\hbar}{2\mu} \int \rho_j(\omega) \coth\left(\frac{\hbar\omega}{2k_B T}\right) \frac{d\omega}{\omega}$$

where μ is the reduced mass, θ_{cD} is the correlated Debye temperature, and the phonon density of states at position R_j is⁴²

$$\rho_j = \frac{3\omega_D^2}{\omega_D^3} \left[1 - \frac{\sin(\omega R_j/c)}{\omega R_j/c} \right] \quad (6)$$

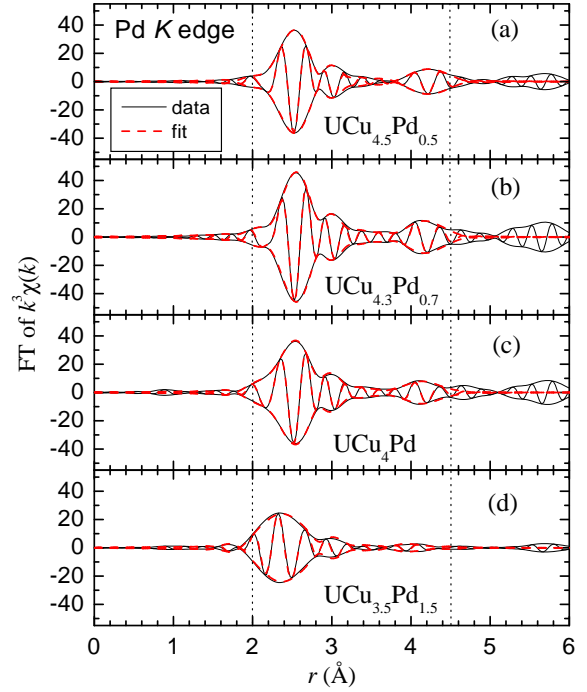
in which ω_D is the usual Debye frequency and $c = \omega_D/k_D$. The expression in brackets of Eq. 6 takes into account the correlated motion of the atom pair. These values of the static disorder σ_{static}^2 can then be compared to those (σ_{KDM}) necessary for the KDM to describe the magnetic susceptibility data. Debye-Waller factors for the neighbors further than the nearest neighbor U-Cu pairs are judged to be less reliable for the purpose of determining σ_{static}^2 , either because the fraction of the amplitude of the peak in the Fourier transform of the XAFS data due to the pair of interest is less than 50% of the peak height (as is the case for the next-neighbor U-Pd/Cu pairs at about 3.1 Å) or simply because the correlated-Debye model does not work very well for further neighbors.³¹

B. Pd K edge

The FT of $k^3\chi(k)$ of the Pd K edge of $\text{UCu}_{5-x}\text{Pd}_x$ for various Pd concentrations is shown in Fig. 6. Hereafter, “Pd’” denotes Pd atoms on $16e$ sites, “Pd” denotes Pd atoms on $4c$ sites, “Cu’” denotes Cu atoms on $4c$ sites, and “Cu” denotes Cu atoms on $16e$ sites. The

main peak at ~ 2.4 Å (peaks in the XAFS transforms are shifted from the real bond lengths due to the phase shifts of the absorbing and backscattering atoms) arises mainly from the large number of Pd-Cu bonds at 2.93 Å with additional contributions (shoulders) from the Pd'-Cu/Pd'-Pd' bonds at 2.50 Å and Pd-U bonds at 3.06 Å with appropriate weights governed by the amount of site interchange s . The main peak at ~ 2.4 Å shifts to lower r with increasing Pd concentration, indicating more of the 16e sites are being occupied by Pd (a situation which must occur for $x > 1$). The model used to fit these data is extended over the basic model used in Ref. 23 by including all Pd bonds, both on the 4c sites and the 16e sites, out to pair distances of 4.59 Å. These fits are tightly constrained in order to reduce the number of fit parameters to be well within Stern's rule.⁴³ For instance, amplitudes for all the peaks are set by only three parameters: S_0^2 , x , and s , with a single S_0^2 used for all data at a given edge and x fixed to the nominal value. In addition, pair distances that are nominally the same, such as $R(\text{Pd}-\text{Cu})$ at 2.93 Å in the nominal structure and $R(\text{Pd}'-\text{Cu}')$ that occurs from the site interchange, are held equal in the fits. Different atom pairs with equal pair distances also have the ratio of the Debye-Waller factors σ^2 held to the ratio of their reduced masses, although this does not account for differences in the correlated Debye temperatures of the various bonds. Finally, a single S_0^2 and threshold energy shift ΔE_0 are used for all bonds and all temperatures. With these constraints we include 15 atom pairs in the fits while only requiring 10 fit parameters from 1.5-4.5 Å, using a k -space window of 2.5-15 Å⁻¹ (Gaussian narrowed by 0.3 Å⁻¹). The value of S_0^2 for the Pd K edge data is determined to be 0.85 ± 0.04 . Representative fits for various Pd concentrations are displayed in Fig. 6 and summarized in Table II. The quality of the fits is quite good with $R \sim 3 - 10\%$ for all Pd concentrations measured and the bond lengths are consistent with diffraction results.

The amount of site interchange s vs x is shown in Fig. 7a along with the nominal values of s , in which the 4c (nominal Pd) sites are filled with Pd up to $x = 1$ (i.e., $s = 0$), and thereafter the Pd atoms begin occupying the 16e (nominal Cu) sites (i.e., $s > 0$). These results indicate that site interchange exists even for low Pd concentrations (results listed in Table III). In a previous XAFS study of UCu₄Pd, the amount of Pd/Cu site interchange was found to be $s = 0.24(3)$.²³ In the present investigation, the data have been analyzed using a more sophisticated model of the local Pd environment (i. e. including further neighbors with site interchange out to 4.6 Å instead of 3.4 Å²³) to obtain $s = 0.32(5)$. While there is a small discrepancy between the two models, the values are consistent with each other within the error bars. Differences in the value of S_0^2 between the two studies may account for this discrepancy. In the present study, the value of the XAFS scale factor $S_0^2 = 0.85$ is based upon a number of Pd concentrations and therefore is judged to be more reliable.



E. D. Bauer et al., Fig. 6

FIG. 6: Fourier transforms of $k^3\chi(k)$ of the Pd K edge data from selected UCu_{5-x}Pd_x samples. The outer envelope is the amplitude and the oscillating inner line is the real part of the complex transform. Solid lines are data for a) $x = 0.5$ (20 K), b) $x = 0.7$ (15 K), c) $x = 1.0$ (3.3 K), and d) $x = 1.5$ (15 K) along with fits (dashed lines) as described in the text. These and all subsequent transforms are from $k=2.5-15$ Å⁻¹ and Gaussian narrowed by 0.3 Å⁻¹. The fit range is from 1.5 to 4.5 Å (dotted lines).

An alternative (equivalent) description of the site interchange from s and x uses the occupancy fractions, defined as follows: f_{4c}^{Pd} and f_{16e}^{Cu} are the fraction of 4c and 16e sites occupied by Pd and Cu, respectively, which are given by:

$$\begin{aligned} f_{4c}^{\text{Pd}} &= x(1 - s) \\ f_{16e}^{\text{Cu}} &= 1 - \frac{sx}{4}. \end{aligned}$$

These occupancy fractions are shown in Fig. 7b. The fits are less sensitive to the parameter f_{16e}^{Cu} due to the relative abundance of 16e sites. The amount of site interchange is roughly constant up to $x = 0.7$ at $s \sim 0.2$ and then increases monotonically to a value of $s \sim 0.4$ at $x = 1.5$. Therefore, it is possible that the system may be furthest away from random occupancy of Pd at $x = 0.7$, given that a minimum in s exists at that concentration. For $x > 0.7$, an increasing number of Pd atoms are located on the smaller 16e sites which is accompanied by an increase of the lattice parameter.^{14,44} Note that the

TABLE II: Fit results of the site interchange model to some of the Pd K edge data from $\text{UCu}_{5-x}\text{Pd}_x$. N —nominal number of neighbors in ordered UCu_4Pd ; A —peak amplitude; σ^2 —square of Debye-Waller factor; R —bond length; f_{16e}^{Cu} —16e site occupancy of Cu; f_{4c}^{Pd} —4c site occupancy of Pd. The site-interchange ions are denoted with a prime, e.g., Pd' is a Pd ion on a nominal Cu (16e) site. The amplitudes of the peaks A are fixed by the amount of Pd/Cu site interchange s and the site occupancy factors f_{16e}^{Cu} and f_{4c}^{Pd} . Atom pairs in parentheses are completely constrained by the pair above them in the table. Debye-Waller factors for pairs with similar bond lengths are also constrained. See Sec. IV B for details. S_0^2 is determined to be 0.85 ± 0.04 . The errors in σ are estimated to be 5% for nearest neighbor bonds and 10% for further neighbor bonds. The errors in R are estimated to be 0.01 Å for nearest neighbor bonds and 0.02 Å for further neighbor bonds.

Pd Concentration x , T		0.7, 15 K			1.0, 3.3 K			1.25, 15 K		
Bond	A constraint	A	σ^2 (Å ²)	R (Å)	A	σ^2 (Å ²)	R (Å)	A	σ^2 (Å ²)	R (Å)
Pd'—Cu	$6S_0^2 s f_{16e}^{Cu}$	0.84	0.0029	2.55	1.50	0.0028	2.56	1.71	0.0025	2.55
(Pd'—Pd')	$6S_0^2 s (1 - f_{16e}^{Cu})$									
Pd'—Cu'	$3S_0^2 s (1 - f_{4c}^{Pd})$	0.18	0.0030	2.91	0.26	0.0025	2.90	0.22	0.0025	2.88
(Pd'—Pd)	$3S_0^2 s f_{4c}^{Pd}$									
(Pd'—U)	$3S_0^2 s$									
Pd—Cu	$12S_0^2 (1 - s) f_{16e}^{Cu}$	8.21	0.0030	2.91	6.38	0.0025	2.90	5.57	0.0025	2.88
(Pd—Pd')	$12S_0^2 (1 - s) (1 - f_{16e}^{Cu})$									
Pd—U	$4S_0^2 (1 - s)$	2.82	0.0025	3.05	2.32	0.0019	3.05	2.11	0.0027	3.05
Pd'—Cu	$12S_0^2 s f_{16e}^{Cu}$	1.68	0.0025	4.31	3.00	0.0036	4.31	3.41	0.0039	4.32
(Pd'—Pd')	$12S_0^2 s (1 - f_{16e}^{Cu})$									
Pd'—Cu'	$4S_0^2 s (1 - f_{4c}^{Pd})$	0.24	0.0051	4.58	0.35	0.0058	4.57	0.29	0.0065	4.55
(Pd'—U)	$4S_0^2 s$									
(Pd'—Pd)	$4S_0^2 s f_{4c}^{Pd}$									
Pd—Cu	$16S_0^2 (1 - s) f_{16e}^{Cu}$	10.95	0.0051	4.58	8.51	0.0058	4.57	7.43	0.0065	4.55
(Pd—Pd')	$16S_0^2 (1 - s) (1 - f_{16e}^{Cu})$									

TABLE III: Amount of Pd/Cu site interchange s for various Pd concentrations x of $\text{UCu}_{5-x}\text{Pd}_x$ determined from fits of the site interchange model to the Pd K edge and U L_{III} edge data. These results from the U-edge data are only reliable as a consistency check on the Pd-edge results (see Sec. IV C). Errors in the last digit are given in parentheses.

x	s	
	Pd K edge	U L_{III} edge
0.3	0.3(1)	0.8(7)
0.5	0.25(3)	0.4(4)
0.7	0.17(3)	0.25(5)
0.9	0.26(4)	0.35(9)
1.0	0.32(5)	0.39(4)
1.25	0.38(4)	0.40(8)
1.5	0.41(3)	0.41(3)

f_{4c}^{Pd} occupancy fractions exhibit a pronounced change in slope close to $x = 0.7$.

C. U L_{III} edge

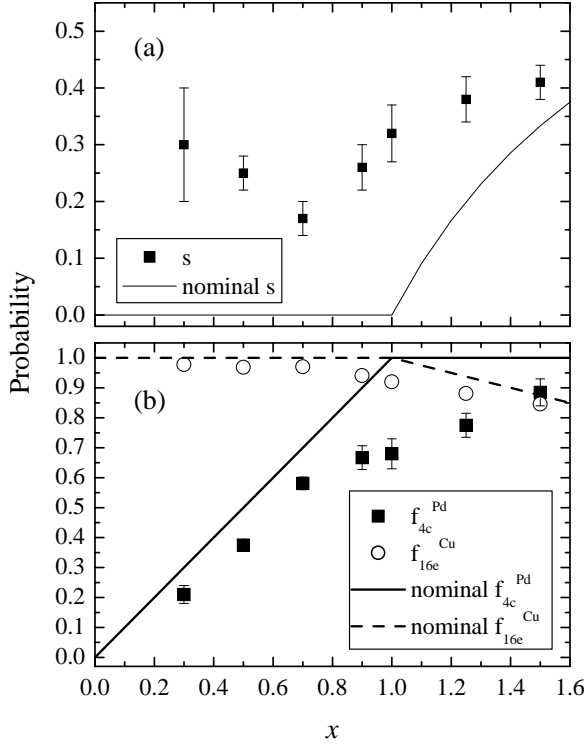
The Pd/Cu site interchange determined from the Pd K edge is introduced into the model for the U L_{III} edge data by fixing the relative amplitudes of the various U—Cu and U—Pd bonds. Constraints on the fits to the U L_{III} data were chosen in a similar manner to the Pd edge constraints, fitting in r -space to pairs as long as 5.0 Å, including 7 pairs but only 8 fit parameters. Represen-

tative fits to the data are shown in Fig. 8 and summarized in Table IV. The value of S_0^2 was determined to be 0.80 ± 0.05 . In order to extract the static continuous disorder, the square of the Debye Waller factor for the U—Cu bond at 2.93 Å $\sigma_{\text{U—Cu}}^2(T)$ was fit to a correlated-Debye model given by Eq. 5.⁴¹ The fits to this model are shown in Fig. 9 for various concentrations of $\text{UCu}_{5-x}\text{Pd}_x$ and the results are collected in Table IV. All measurements of $\sigma_{\text{U—Cu}}^2$ are consistent with zero disorder, as was found in the YbXCu_4 ($X = \text{Ag, Cd, In, Tl}$) series.³³

As a consistency check for the amount of site interchange, the U L_{III} edge data were fit with s as a free parameter, but subject to the relative amplitude constraints of the peaks given by the site interchange model. The values of s obtained in this manner are only used to provide a qualitative comparison to those value determined from the Pd edge data since the results of the U edge fits are much more model dependent (i.e. the U—Cu and U—Pd' pair distances are constrained to each other) and some parameters are strongly correlated with one another (i. e. s and the near neighbor Debye-Waller factors). The results of these fits are inconclusive for $x \leq 0.5$ due to the small amplitudes of the bonds involving site interchange, but compare quite favorably with the values obtained solely from the Pd edge for $x > 0.5$ (results listed in Table III).

TABLE IV: Fit results of the site interchange model to some of the U L_{III} edge data of $UCu_{5-x}Pd_x$. Definitions and constraints are similar to those in Table II. S_0^2 is determined to be 0.80 ± 0.05 .

Pd Concentration x , T		0.7, 15 K			1.0, 3.3 K			1.25, 15 K		
Bond	A constraint	A	σ^2 (\AA^2)	R (\AA)	A	σ^2 (\AA^2)	R (\AA)	A	σ^2 (\AA^2)	R (\AA)
U–Cu	$12S_0^2 f_{16e}^{Cu}$	9.31	0.0011	2.91	8.83	0.0021	2.92	8.46	0.0019	2.93
(U–Pd')	$12S_0^2 (1 - f_{16e}^{Cu})$									
U–Cu'	$4S_0^2 f_{4c}^{Pd}$	1.86	0.0015	3.04	2.18	0.0020	3.05	2.48	0.0042	3.07
(U–Pd)	$4S_0^2 (1 - f_{4c}^{Pd})$									
U–Cu	$16S_0^2 f_{16e}^{Cu}$	12.42	0.0027	4.56	11.78	0.0035	4.57	11.28	0.0032	4.59
(U–Pd')	$16S_0^2 (1 - f_{16e}^{Cu})$									
U–U	$12S_0^2$	9.60	0.0022	4.97	9.60	0.0028	4.99	9.60	0.0030	5.00

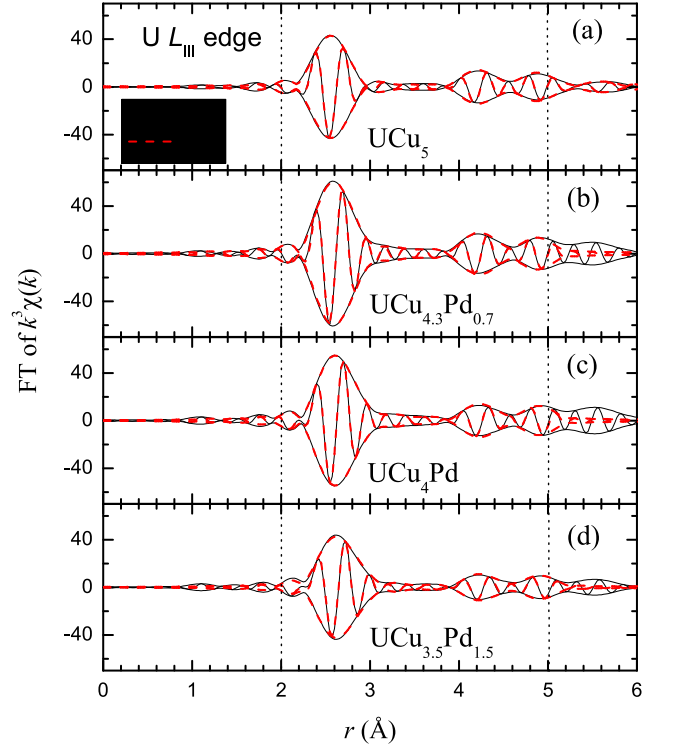


Bauer et al., Fig 7

FIG. 7: Panel a) shows the amount of Pd/Cu site interchange s vs Pd concentration x in $UCu_{5-x}Pd_x$ determined from fits of the Pd K edge data to the site interchange model. The nominal s is based on a simple model in which the Pd atoms first fill the $4c$ sites for $x < 1$ and thereafter fill the $16e$ sites. Panel b) gives the occupancy fractions f_{4c}^{Pd} (fraction of Pd on $4c$ sites) and f_{16e}^{Cu} (fraction of Cu on $16e$ sites) vs x . The nominal occupancy factors f_{4c}^{Pd} and f_{16e}^{Cu} are indicated by the solid and dashed lines, respectively.

D. Cu K edge

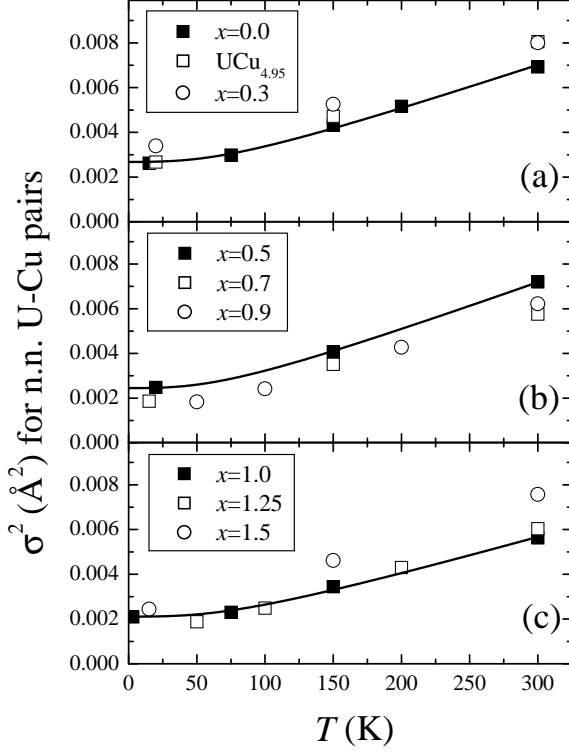
The FT of $k^3\chi(k)$ of the Cu K edge of $UCu_{5-x}Pd_x$ for various Pd concentrations is shown in Fig. 10. The main peak at ~ 2.3 \AA is shifted to lower r relative to the peak in the Pd K edge data due to the larger number



E.D. Bauer et al., Fig. 8

FIG. 8: Fourier transforms of $k^3\chi(k)$ of the U L_{III} edge data from selected $UCu_{5-x}Pd_x$ samples. Solid lines are data for a) $x = 0$ (15 K), b) $x = 0.7$ (15 K), c) $x = 1.0$ (3.3 K), and d) $x = 1.5$ (15 K) along with fits (dashed lines). The fit range is from 2.0 to 5.0 \AA (dotted lines).

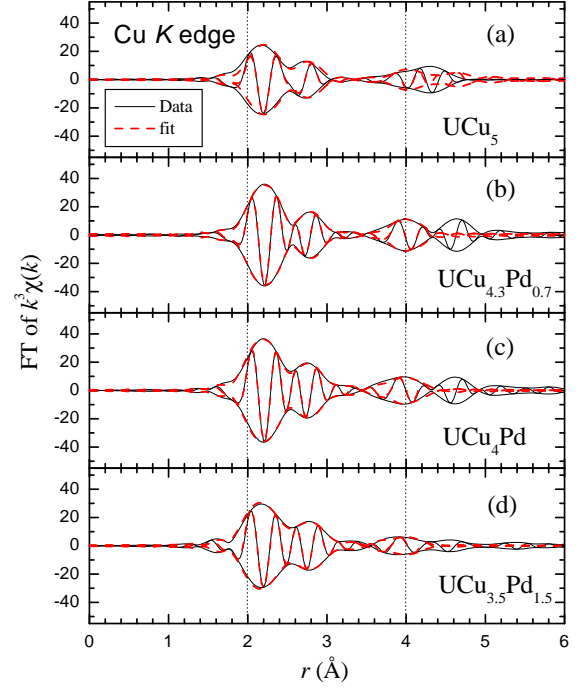
of Cu–Cu bonds at 2.50 \AA . The Cu K edge data were also fit by the site interchange model using similar amplitude constraints involving s , x , and S_0^2 . The value of S_0^2 is determined to be 0.61 ± 0.06 . Due to the abundance of Cu present in the $UCu_{5-x}Pd_x$ specimens, the fits are not very sensitive to the site interchange parameter s for the relatively low Pd concentrations considered here. The fits of this model to the Cu K edge data using the values of s obtained from the Pd K edge are shown in Fig. 10. A quantitative comparison can be made to the Pd K and U L_{III} edge data for those peaks which



Bauer et al., Fig. 9

FIG. 9: Square of the Debye-Waller factor of the U-Cu bond at 2.93 \AA $\sigma_{\text{U-Cu}}^2$ vs T of $\text{UCu}_{5-x}\text{Pd}_x$ determined from the U L_{III} edge fits. Panel a): $\text{UCu}_{4.95}$, $x = 0$, and $x = 0.3$; panel b) $x = 0.5$, $x = 0.7$, and $x = 0.9$; panel c) $x = 1.0$, $x = 1.25$, and $x = 1.5$. A typical fit to the correlated Debye model is indicated by the solid line for $x = 0$, $x = 0.5$, and $x = 1.0$ in panels a), b), and c), respectively.

dominate the Cu K edge spectra. In general, there is good agreement between the Cu edge fit results and the Pd and U edge results. However, the details of the fit parameters for some peaks with small amplitudes are only in qualitative agreement with the fits to the other edge data. For instance, the Debye-Waller factors of the Cu-Pd' peak of the $x = 0.7$ sample ($\sigma^2 = 0.0012 \text{ \AA}^2$) and Pd'-Cu peak ($\sigma^2 = 0.0029 \text{ \AA}^2$) at 2.5 \AA as well as the bonds lengths ($R = 2.48 \text{ \AA}$ for Cu-Pd' vs $R = 2.55 \text{ \AA}$ for Pd'-Cu) are somewhat different. The difference in the Debye-Waller factors is likely due to the particular choice of constraints used in fitting the Cu edge data to the site interchange model, i.e., the Debye-Waller factor of the Cu-Pd' peak was set by the Cu-Cu peak which has the largest amplitude in the XAFS spectra (see Sec. IV B). Therefore, the Debye-Waller factor of the Cu-Cu peak dominates the fit and its small magnitude could be due to the presence of small amounts of free Cu in some samples causing a lower (incorrect) value for S_0^2 for the Cu edge data. A plausible explanation for the difference in bond lengths of the nearest neighbor bonds is a slight distortion of the Cu tetrahedra as discussed below. Oth-



E.D. Bauer et al., Fig. 10

FIG. 10: Fourier transforms of $k^3\chi(k)$ of the Cu K edge data from selected $\text{UCu}_{5-x}\text{Pd}_x$ samples. Solid lines are data for a) $x = 0$ (15 K), b) $x = 0.7$ (20 K), c) $x = 1.0$ (20 K), and d) $x = 1.5$ (15 K) along with fits (dashed lines). The fit range is from 2.0 to 4.0 \AA (dotted lines).

erwise, the fit parameters obtained from the Cu K edge data are consistent with the other edges and so are not reported in detail here.

V. CONSEQUENCES OF MEASURED LATTICE DISORDER ON V AND T_K

The distribution of hybridization strengths $P(V)$ for UCu_4Pd is shown in Fig. 11 using the measured value of $\sigma_{\text{static}}^2 = 0.0002 \text{ \AA}^2$ obtained from the U L_{III} edge data along with the curves for one standard deviation of this value ($\sigma_{\text{static}}^2 = 0 \text{ \AA}^2$ (binomial) and $\sigma_{\text{static}}^2 = 0.00078 \text{ \AA}^2$). The value of $\sigma_{\text{static}}^2 = \sigma_{\text{KDM}}^2 (= 0.00343 \text{ \AA}^2)$ necessary to fit the $\chi(T)$ data with the KDM model produces a distribution that is considerably broader than the one derived from the measured amount of static disorder. The mean hybridization $\langle V \rangle$ for all Pd concentrations was calculated using the measured values of s and σ_{static}^2 and is shown in Fig. 11a along with the spread in hybridization strengths $\Delta V / \langle V \rangle$ (Fig. 11b). The average hybridization strength increases linearly with increasing Pd concentration reflecting the additional hybridization

TABLE V: Comparison of measured and calculated static continuous disorder in $\text{UCu}_{5-x}\text{Pd}_x$. The parameters σ_{static}^2 and θ_{cD} were determined from fits to the U L_{III} edge Debye-Waller factors to a correlated Debye model. The values of the static disorder necessary to fit the magnetic susceptibility σ_{KDM}^2 are determined from fits of the Kondo disorder model to the $\chi(T)$ data. Errors in the last digit are given in parentheses.

x	σ_{U-Cu}^2 (\AA^2)	θ_{cD} (K)	σ_{static}^2 (\AA^2)	σ_{KDM}^2 (\AA^2)
$\text{UCu}_{4.95}$	0.0027(3)	290(4)	0.0004(3)	
0	0.0026(3)	318(7)	0.0006(3)	
0.3	0.0034(3)	310(8)	0.0013(3)	
0.5	0.0025(4)	306(10)	0.0003(4)	
0.7	0.0011(3)	335(15)	0.0000(3)	
0.9	0.0018(4)	314(2)	-0.0005(4)	0.0038
1.0	0.0021(6)	345(7)	0.0002(6)	0.0030
1.25	0.0019(3)	322(4)	-0.0003(3)	0.0028
1.5	0.0023(6)	300(7)	0.0003(6)	0.0028

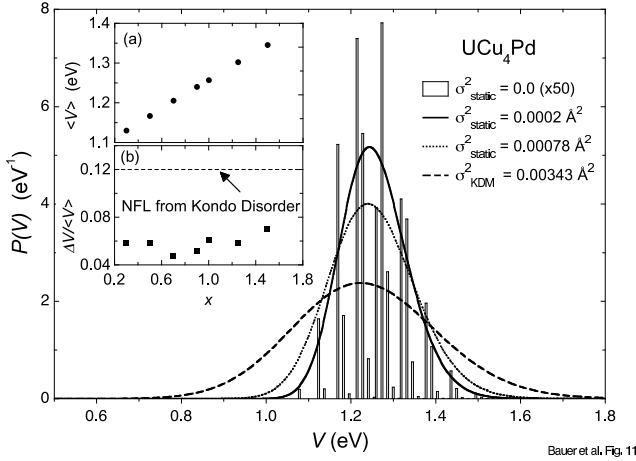


FIG. 11: Distribution of hybridization strengths $P(V)$ for UCu_4Pd . The solid curve is the distribution using the measured value of σ_{static}^2 obtained from the U L_{III} edge data along with the distributions within one standard deviation of the measured value of σ_{static}^2 (dotted line). The dashed line uses the value of σ_{KDM}^2 necessary to fit the $\chi(T)$ data with the KDM model. Inset a): Average hybridization $\langle V \rangle$ vs x . Inset b): Spread from hybridization strengths $\Delta V / \langle V \rangle$ vs x .

due to the larger Pd atoms, while the width of the distribution increases only slightly.

The values of the square of the Debye-Waller factor σ_{static}^2 , determined from the U L_{III} edge data for the U-Cu bond at 2.93 \AA , are compared to those values of the static disorder needed to fit the $\chi(T)$ data using the KDM and are displayed in Fig. 12. The amount of the measured continuous static disorder is small and consistent with zero disorder. The value of σ_{static}^2 for $x = 0.3$ is larger than for the other concentrations. This anomaly may be attributed to the influence of sample oxidation since no special care was taken to minimize oxidation in this compound as was the case for UCu_5 and $\text{UCu}_{4.95}$.

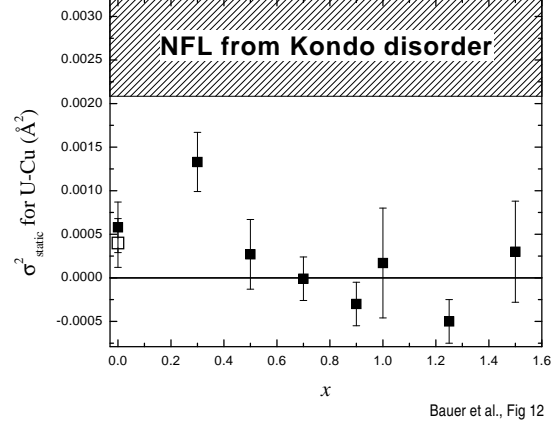


FIG. 12: The static part of the bond-length distribution variance for the U-Cu bond at ~ 2.93 \AA , σ_{static}^2 vs x of $\text{UCu}_{5-x}\text{Pd}_x$. Data for the $\text{UCu}_{4.95}$ sample is denoted by the open square. The shaded area is the approximate amount of disorder necessary to fully explain NFL behavior in $\text{UCu}_{5-x}\text{Pd}_x$ compounds based on a distribution of hybridization strengths generated by lattice disorder.

samples. However, no trace of UO_2 was found in the U L_{III} XAFS spectra. The amount of static disorder used to reproduce the logarithmic divergence in the magnetic susceptibility with the KDM σ_{KDM}^2 is indicated by the shaded region in Fig. 12, reflecting the uncertainty in comparing the model with the experimental data. The lower bound on σ_{KDM}^2 is estimated to be 20% below the smallest value of σ_{KDM}^2 ($x = 1.5$).

VI. DISCUSSION

In our previous XAFS study on UCu_4Pd , Pd/Cu site interchange was found to occur, providing evidence that *chemical* disorder exists in this compound.²³ We suggested from these results that lattice disorder is the microscopic origin of the Kondo disorder model and therefore, produces the observed NFL characteristics. However, a necessary assumption for this lattice origin of the KDM was the inclusion of bond-length disorder (at that time unquantifiable), presumably caused by the site interchange. This assumption is tested in the present investigation by employing an experimental determination of the static continuous disorder about the U atoms (Fig. 12) for a number of different Pd concentrations. These σ_{static}^2 results are obtained from a more sophisticated fitting model of the local Pd environment and are compared to those values of σ_{KDM}^2 necessary to explain the NFL properties of $\text{UCu}_{5-x}\text{Pd}_x$ ($x = 0.9 - 1.5$) via the Kondo disorder model. This comparison was not possible in the original work²³ because the fitting model was not complete enough and there were not any data on other Pd concentrations, making a determina-

tion of certain relevant experimental parameters (especially S_0^2) less reliable. Our results in the present study indicate that while Pd/Cu site interchange exists for all Pd concentrations measured, it does not produce enough static continuous disorder to explain the non-Fermi liquid behavior observed in the magnetic susceptibility (and presumably the specific heat) *within the variant of the Kondo disorder model discussed here*, i.e. the KDM with a distribution of T_K s produced by lattice disorder in the hybridization strength V . It is important to emphasize this last caveat since other sources of disorder aside from a distribution of hybridization strengths due to bond length disorder, such as a distribution of the density of states or f -ion energies, could cause a distribution of Kondo temperatures. Although the relationship between the *local* density of states (the relevant quantity) and that derived from band structure calculations is unclear since these calculations are usually done in the clean limit (i.e., no disorder), fluctuations in the local density of states are a real concern given the shape of the d -level density with energy expected from band structure calculations on YbCu₄Pd.³⁶ Moreover, the tight-binding model for the hybridization treats all the near neighbor U-Cu atom pairs equivalently, and therefore does not include potential phase differences that may occur in the presence of disorder, possibly broadening the distribution of T_K s.⁴⁵ Therefore, the Kondo disorder model may still apply to UCu_{5-x}Pd_x if other disorder effects are the dominant sources of Kondo disorder other than a distribution of hybridization strengths due to bond length disorder. An explanation for the presence of site interchange, yet lack of a spread in U-M bond lengths, is that site interchange causes a distortion in the Cu tetrahedra which is roughly perpendicular to the U-Pd' or U-Cu bonds. Support for this scenario is provided by the difference in the bond lengths of the Pd'-Cu ($R \sim 2.54$ Å) and Cu-Pd' ($R \sim 2.48$ Å) observed for all Pd concentrations. The variation in the U-Pd' bond length due to this distortion is small, i.e., $\Delta R \sim [(2.93 \text{ Å})^2 + (0.06 \text{ Å})^2]^{1/2} - 2.93 \text{ Å} \sim 0.0006 \text{ Å}$.

A recent calculation that incorporates local fluctuations in the density of states, ϵ_f , and V into a disordered Anderson lattice model with ≈ 200 sites has been performed by Miranda and Dobrosavljević.^{21,22} Their results indicate the presence of Griffiths' singularities (not associated with the proximity to magnetic order^{16,17}), giving rise to NFL behavior near a metal-insulator transition; the NFL behavior was found to exist for all three types of disorder mentioned above over a broad range of values of those parameters.^{21,22} In this model, the presence of disorder will cause a variation in the magnitude of the conduction electron wavefunctions leading to a spread in the density of states. Therefore, even a discrete distribution of hybridization strengths due to site interchange alone (or a small amount of continuous disorder) will, in principle, give rise to Griffiths' singularities and NFL behavior within this disordered Anderson lattice model. However, calculations within this model starting from a

discrete distribution of hybridizations similar to that in Fig. 11 do not generate enough width to the density of states to explain the NFL behavior.⁴⁶

While there is some supporting evidence for the applicability of the Kondo disorder model to UCu_{5-x}Pd_x,^{10,13} more recent studies,^{24,26,47,48} in addition to this one, suggest other non-Fermi liquid models may be more appropriate. For instance, even though the specific heat of annealed samples of UCu₄Pd exhibit a NFL-like logarithmic divergence, the electrical resistivity no longer displays a linear T -dependence, clearly at odds with the predictions of the Kondo disorder model.²⁴ In addition, while the Cu spin-lattice relaxation rates $1/T_1$ of UCu_{3.5}Pd_{1.5} in magnetic fields below $H = 5$ T are consistent with the KDM,^{25,48} $1/T_1$ in higher magnetic fields up to $H = 9$ T is not well described by this model.⁴⁸ Recent μ SR measurements²⁶ on UCu₄Pd and UCu_{3.5}Pd_{1.5} reveal that the muon relaxation rates are two orders of magnitude faster than what is expected from the KDM. There is growing evidence from NMR,¹³ μ SR,²⁶ and inelastic neutron scattering experiments⁴⁷ that short-range magnetic correlations (less than a unit cell distance) are present in UCu_{5-x}Pd_x. One possible explanation for these magnetic correlations is the formation of magnetic clusters in the vicinity of a quantum critical point in a disordered material, similar to the scenario proposed by Castro Neto and coworkers.^{16,17} The spin glass behavior observed^{20,27} in the $x = 1$ and $x = 1.5$ samples at $T_f \sim 0.2 - 0.3$ K could be due to the freezing of these magnetic clusters in this picture. The power law behavior of the specific heat and magnetic susceptibility of such compounds and other Ce- and U-based materials^{19,20} is consistent with this Griffiths' phase model. However, the Griffiths' phase predictions of the dynamics of the magnetic correlations do not agree with the inelastic neutron and μ SR measurements, which are perhaps best viewed within a framework of a quantum critical point scenario in which spin glass^{49,50} or antiferromagnetic order^{7,8,9,51} has been suppressed to $T = 0$ K. Moreover, it is not clear whether the observed magnetic correlations⁴⁷ are strong enough to allow for the Griffiths' phase model. Clearly, the theoretical understanding of this system is far from complete.

An investigation²⁴ of the effects of annealing on the physical properties of UCu₄Pd was recently reported by Weber and coworkers and provides another way to study the role of disorder in this system. Annealing the samples at 750 °C for 1 and 2 weeks produced a decrease in the lattice parameter a , more consistent with the nearly linear relation^{14,24,35,44} observed (for unannealed samples) between a and x for $x < 0.7$, while splat quenching the sample results in an increase of a , relative to the unannealed sample. One possible interpretation of this behavior is that the unannealed sample has a comparable amount of site interchange to the one studied here and splat quenching gives rise to more site interchange while annealing reduces it. However, note that the lattice parameter of the annealed samples extrapo-

lates to the linear a vs x relation of the unannealed samples below $x=0.7$. Since the unannealed samples have site interchange, even for low Pd concentrations, the annealed $x=1.0$ specimens most likely also have a considerable amount of site interchange. In any case, even though the specific heat divided by temperature of the annealed samples shows a logarithmic dependence over a larger temperature range (0.08-10 K) compared to the unannealed specimens, the electrical resistivity no longer exhibits a linear T -dependence, indicating that the low temperature properties are greatly influenced by disorder. Our results on unannealed samples as shown in Fig. 7 indicate an increase in the site interchange for samples above $x = 0.7$. Therefore, these XAFS results are consistent with the interpretation of Weber *et al.*²⁴ that annealing reduces the site interchange, although it does not suppress it completely. Future work, such as XAFS, μ SR, and neutron scattering measurements on annealed samples of $\text{UCu}_{5-x}\text{Pd}_x$ should continue to provide information that will lead to a better understanding of the interplay between disorder and the NFL properties in this system.

VII. CONCLUSIONS

We have measured the local structure about the U, Cu, and Pd atoms in $\text{UCu}_{5-x}\text{Pd}_x$ ($0 \leq x \leq 1.5$) using the XAFS technique. A model involving Pd/Cu site interchange was used to fit the Pd and Cu K edge and U L_{III} edge data. Pd/Cu site interchange s was found to occur in all samples with a roughly constant value of $s \sim 0.2$ up to $x = 0.7$ and increased to $s \sim 0.4$ at $x = 1.5$. These results were used to determine the static

disorder about the U atoms. The magnetic susceptibility of $\text{UCu}_{5-x}\text{Pd}_x$ was calculated with the Kondo disorder model via a tight binding approximation for the hybridization strength V_{fd} , assuming that lattice disorder is the cause of Kondo disorder. Our results indicate that the measured static disorder due to Pd/Cu site interchange does not produce a sufficient width to the distribution of (tight-binding) V_{fd} to generate NFL behavior within the Kondo disorder model and suggests either that there are sources of Kondo disorder other than a distribution of hybridization strengths with a lattice-disorder origin or that the Kondo disorder model is not applicable to $\text{UCu}_{5-x}\text{Pd}_x$. However, the presence of significant Pd/Cu site interchange should in principle still cause a distribution of hybridization strengths and may well couple to changes in the local electron charge densities, and therefore strongly favor NFL models which include disorder, such as the various Griffiths' phase models.

Acknowledgments

We thank Prof. F. Bridges for assistance in collecting the XAFS data. We also to thank D. E. MacLaughlin, J. M. Lawrence, D. L. Cox, E. Miranda, and E.-W. Scheidt for many useful discussions. This work was partially supported by U. S. National Science Foundation under Grant No. DMR00-72125, the U. S. Department of Energy (DOE) under Grant No. DE FG03-86ER-45230, and by the Office of Basic Energy Sciences (OBES), Chemical Sciences Division of the DOE, Contract No. AC03-76SF00098. XAFS data were collected at the Stanford Synchrotron Radiation Laboratory, which is operated by the DOE/OBES.

-
- ¹ L. D. Landau, Sov. Phys. JETP **3**, 920 (1957).
 - ² M. B. Maple, C. L. Seaman, D. A. Gajewski, Y. Dalichaouch, V. B. Barbetta, M. C. de Andrade, H. A. Mook, H. G. Lukefahr, O. O. Bernal, and D. E. MacLaughlin, J. Low Temp. Phys. **95**, 225 (1994).
 - ³ A. J. Schofield, Contemporary Physics **40**, 95 (1999).
 - ⁴ See, for example, articles in *Proceedings of the Conference on Non-Fermi Liquid Behavior in Metals*, Santa Barbara, California, 1996, edited by P. Coleman, M. B. Maple, and A. J. Millis, J. Phys.: Condens. Matter **8** (1996).
 - ⁵ H. von Löhneysen, J. Magn. Magn. Mat. **200**, 532 (1999).
 - ⁶ G. R. Stewart, Rev. Mod. Phys. **73**, 797 (2001).
 - ⁷ J. A. Hertz, Phys. Rev. B **14**, 1165 (1976).
 - ⁸ A. J. Millis, Phys. Rev. B **48**, 7183 (1993).
 - ⁹ M. A. Continentino, Phys. Rep. **239**, 179 (1994).
 - ¹⁰ O. O. Bernal, D. E. MacLaughlin, H. G. Lukefahr, and B. Andraka, Phys. Rev. Lett. **75**, 2023 (1995).
 - ¹¹ E. Miranda, V. Dobrosavljević, and G. Kotliar, J. Phys.: Condens. Matter **8**, 9871 (1996).
 - ¹² E. Miranda, V. Dobrosavljević, and G. Kotliar, Phys. Rev. Lett. **78**, 290 (1997).
 - ¹³ D. E. MacLaughlin, R. H. Heffner, G. J. Nieuwenhuys, G. M. Luke, Y. Fudamoto, R. Chau, M. B. Maple, and B. Andraka, Phys. Rev. B **58**, R11849 (1998).
 - ¹⁴ B. Andraka and G. R. Stewart, Phys. Rev. B **47**, 3208 (1993).
 - ¹⁵ R. Chau and M. B. Maple, J. Phys.: Condens. Matter **8**, 9939 (1996).
 - ¹⁶ A. H. Castro Neto, G. Castilla, and B. A. Jones, Phys. Rev. Lett. **81**, 3531 (1998).
 - ¹⁷ A. H. Castro Neto and B. A. Jones, Phys. Rev. B **62**, 14975 (2000).
 - ¹⁸ R. B. Griffiths, Phys. Rev. Lett. **23**, 17 (1969).
 - ¹⁹ M. C. de Andrade, R. Chau, R. P. Dickey, N. R. Dille, E. J. Freeman, D. A. Gajewski, M. B. Maple, R. Movshovich, A. H. Castro Neto, G. Castilla, et al., Phys. Rev. Lett. **81**, 5620 (1998).
 - ²⁰ R. Vollmer, T. Pietrus, H. v. Löhneysen, R. Chau, and M. B. Maple, Phys. Rev. B **61**, 1218 (2000).
 - ²¹ E. Miranda and V. Dobrosavljević, Phys. Rev. Lett. **86**, 264 (2001).
 - ²² E. Miranda and V. Dobrosavljević, J. Magn. & Magn. Mater. **226-230**, 110 (2001).
 - ²³ C. H. Booth, D. E. MacLaughlin, R. H. Heffner, M. B.

- Maple, and R. Chau, Phys. Rev. Lett. **81**, 3960 (1998).
- ²⁴ A. Weber, S. Körner, E.-W. Scheidt, S. Kehrein, and G. R. Stewart, Phys. Rev. B **63**, 205116 (2001).
 - ²⁵ B. Ambrosini, J. L. Gavilano, P. Vonlanthen, and H. R. Ott, Phys. Rev. B **60**, R11249 (1999).
 - ²⁶ D. E. MacLaughlin, R. H. Heffner, G. J. Nieuwenhuys, M. S. Rose, J. E. Sonier, B. Andraka, R. Chau, and M. B. Maple (2001), submitted to Phys. Rev. Lett.
 - ²⁷ E. W. Scheidt, T. Schreiner, K. Heuser, S. Koerner, and G. R. Stewart, Phys. Rev. B **58**, R10104 (1998).
 - ²⁸ H. Nakamura, Y. Kitaoka, K. Asayama, Y. Ōnuki, and M. Shiga, J. Phys.: Condens. Matter **6**, 10567 (1994).
 - ²⁹ D. D. Sarma, F. U. Hillebricht, and M. Campagna, Surface Science **162**, 563 (1985).
 - ³⁰ T. M. Hayes and J. B. Boyce, in *Solid State Physics*, edited by H. Ehrenreich, F. Seitz, and D. Turnbull (Academic, New York, 1982), vol. 37, p. 173.
 - ³¹ G. G. Li, F. Bridges, and C. H. Booth, Phys. Rev. B **52**, 6332 (1995).
 - ³² S. I. Zabinsky, J. J. Rehr, A. Ankudinov, R. C. Albers, and M. J. Eller, Phys. Rev. B **52**, 2995 (1995).
 - ³³ J. M. Lawrence, P. S. Riseborough, C. H. Booth, J. L. Sarrao, J. D. Thompson, and R. Osborn, Phys. Rev. B **63**, 054427 (2001).
 - ³⁴ R. Chau, M. B. Maple, and R. A. Robinson, Phys. Rev. B **58**, 139 (1998).
 - ³⁵ S. Körner, A. Weber, J. Hemberger, E. W. Scheidt, and G. R. Stewart, J. Low Temp. Phys. **121**, 105 (2000).
 - ³⁶ P. Monachesi and A. Continenza, Phys. Rev. B **54**, 13558 (1996).
 - ³⁷ W. A. Harrison and G. K. Straub, Phys. Rev. B **36**, 2695 (1987).
 - ³⁸ G. K. Straub and W. A. Harrison, Phys. Rev. B **31**, 7668 (1985).
 - ³⁹ C. H. Booth, E. D. Bauer, M. B. Maple, J. M. Lawrence, G. H. Kwei, and J. L. Sarrao, J. Synchrotron Rad. **8**, 191 (2001).
 - ⁴⁰ V. T. Rajan, Phys. Rev. Lett. **51**, 308 (1983).
 - ⁴¹ E. D. Crozier, J. J. Rehr, and R. Ingalls, in *X-Ray Absorption: Principles, Applications, Techniques of EXAFS, SEXAFS, XANES*, edited by D. Konigsberger and R. Prins (Wiley, New York, 1988), p. 373.
 - ⁴² G. B. Beni and P. M. Platzman, Phys. Rev. B **14**, 1514 (1976).
 - ⁴³ E. A. Stern, M. Qian, Y. Yacoby, S. M. Heald, and H. Maeda, Physica C **209**, 331 (1993).
 - ⁴⁴ R. Chau, Ph.D. thesis, University of California, San Diego (1997).
 - ⁴⁵ D. L. Cox (2002), private communication.
 - ⁴⁶ E. Miranda (2002), private communication.
 - ⁴⁷ M. C. Aronson, R. Osborn, R. Chau, M. B. Maple, B. D. Rainford, and A. P. Murani (2001), submitted to Phys. Rev. Lett.
 - ⁴⁸ N. Büttgen, W. Trinkl, J.-E. Weber, J. Hemberger, A. Loidl, and S. Kehrein, Phys. Rev. B **62**, 11545 (2000).
 - ⁴⁹ S. Sachdev, Phil. Trans. R. Soc. London A **356**, 173 (1998).
 - ⁵⁰ R. G. Grepel and M. J. Rozenberg, Phys. Rev. B **60**, 4702 (1999).
 - ⁵¹ A. J. Millis, P. B. Littlewood, and B. I. Shraiman, Phys. Rev. Lett. **74**, 5144 (1995).